HHS Public Access

Author manuscript

Radiat Res. Author manuscript; available in PMC 2019 July 01.

Published in final edited form as:

Radiat Res. 2018 July ; 190(1): 63–71. doi:10.1667/RR15007.1.

Cortical Thinning and Structural Bone Changes in Non-human Primates Following Single Fraction Whole Chest Radiation

Michael Farris, MD[1], **Emory R. McTyre, M.D.**[1], **Catherine Okoukoni, Ph.D.**[1,2], **Greg Dugan, DVM**[3], **Brendan J. Johnson, B.S.A.**[4], **William Blackstock, M.D.**[1], **Michael T. Munley, PhD**[1,2,5], **J. Daniel Bourland, Ph.D.**[1,5], **J. Mark Cline, DVM, Ph.D**[3], and **Jeffrey S. Willey, Ph.D.**[1]

[1]Department of Radiation Oncology, Wake Forest University School of Medicine, Winston-Salem, North Carolina USA

[2]Department of Biomedical Engineering, Wake Forest University School of Medicine, Winston-Salem, North Carolina USA

[3]Department of Pathology/Section on Comparative Medicine, Wake Forest University School of Medicine, Winston-Salem, North Carolina USA

[4]Department of Veterinary Medicine and Surgery, College of Veterinary Medicine, University of Missouri

[5]Department of Physics, Wake Forest University School of Medicine, Winston-Salem, North Carolina USA

Abstract

Stereotactic body radiation therapy (SBRT) is associated with an increased risk of vertebral compression fracture (1–5). While bone is typically considered radiation-resistant, fractures frequently occur within the first year of SBRT (6–11). Our purpose was to determine if rapid deterioration of bone occurs in vertebrae post-irradiation (IR). Sixteen male rhesus macaques non-human primates (NHPs) were analyzed after total chest irradiation (IR) to a midplane dose of 10 Gy. Ages at IR varied from 45 – 134 mo. Computed tomography (CT) scans were taken 2 mo prior to IR and 2, 4, 6, and 8 mo post-IR for all animals. Bone mineral density (BMD) and cortical thickness (Ct.Th) were calculated longitudinally for thoracic (T)9, lumbar (L)2, and L4 vertebral bodies; gross morphology and histopathology were assessed per vertebra. Greater mortality (related to pulmonary toxicity) was noted in NHPs < 50 mo at time of IR vs NHPs > 50mo ($p = 0.03$). Animals older than 50 mo at IR lost Ct.Th in T9 by 2 mo post IR ($p = 0.0009$), which persisted to 8 mo. In contrast, no loss of Ct.Th was observed in vertebrae out-of-field (L2 and L4). Loss of BMD was observed by 4 mo post-IR for T9, and 6 mo post IR for L2 and L4 ($p < 0.01$). For NHPs younger than 50 mo at IR, both Ct.Th and BMD decreased in T9, L2, and L4 by 2 mo post-IR ($p < 0.05$). Regions that exhibited the greatest degree of cortical thinning as determined from CT scans also exhibited increased porosity histologically. Rapid loss of Ct.Th was observed after high dose chest IR in NHPs. Younger age at IR was associated with increased pneumonitis related mortality, as well as greater loss of both BMD and Ct.Th at both in-and out-of-field

Corresponding Author: Jeffrey Willey, 412 NRC Building, Wake Forest School of Medicine, Winston-Salem, NC 27157, Phone: (336) 713-7637, jwilley@wakehealth.edu.

vertebrae. Older NHPs exhibited rapid loss of BMD and Ct.Th from in-field vertebrae, but only loss of BMD in out of field vertebrae. Bone is sensitive to high dose radiation, and rapid loss of bone structure and density could facilitate fractures.

Introduction

Radiation therapy (RT) is a risk factor for bone morbidity and fracture (12–15). Vertebral RT significantly increases the risk of post-treatment vertebral compression fracture (VCF) (1–5). Acute structural bone changes have been reported following pelvic (13), lumbar spine (16, 17), and thoracic RT (6), however clinically relevant data on this topic is currently limited.

Bone mineral density (BMD) and cortical thickness (Ct.Th) are two of the primary metrics used to quantitatively describe bone structural changes and predict for fracture risk (6, 18, 19). The severity of RT-induced structural changes appears be impacted by both dose and age at irradiation (17, 20, 21). Wei et al. showed that doses as low as 5 Gy correlated with significant BMD loss (>20%) within just 4 months of irradiation (IR), and this effect was persistent at 9 month follow-up (17). While data regarding acute changes in BMD post-RT from clinical studies is limited, literature describing the acute changes in Ct.Th post-RT that could predispose to fracture are nearly absent (13). This is due to limitations in conventional computed tomography (CT) resolution of follow-up scans. Both decreased Ct.Th and BMD may predispose those at highest risk of VCF towards progression and collapse with symptoms (22). Early identification of those at highest risk for RT induced bone changes could potentially allow for better selection for prophylactic interventions(15). The effects of RT are difficult to study using clinical data alone due to numerous confounding factors. These factors include chemotherapy,(23) steroids,(24) reduced mobility,(25) and direct bony infiltration by tumor,(26, 27) which are all detrimental to bone health.

Non-human primates are a good model for studying bone related changes that can be translated to expected responses in humans. These NHPs exhibit both changes of normal aging and response to fractionated RT that is well correlated with what has been shown in humans (28–31). In the present study, we assessed the subacute, longitudinal effects of IR on vertebral structural properties (e.g., Ct.Th and BMD) in rhesus macaques non-human primates (NHPs) when irradiated prior to or after skeletal maturity. Our goal was to determine if rapid deterioration of bone occurs in vertebrae of NHPs post-irradiation (IR) that we could assess using our cortical thickness and dose mapping approach for measuring longitudinal architectural and density changes.

Methods

Subjects

Sixteen male rhesus monkeys (Macaca mulatta) were exposed to uniform total chest irradiation using anterior-posterior parallel-opposed 6 MV x-ray beams. At time of IR the ages of the non-human primates (NHPs) ranged from 45 – 134 months old with a median of 57 months (young adults). Weights at time of IR ranged from 4.4–11.25 kg. These subjects

were randomized into one of two treatment groups, either saline (n=7) or superoxide dismutase (SOD) mimetic “Hexyl”, a potential mitigator of radiation injury in lung (n=9, 0.125 mg/kg in a saline vehicle)(32). Increased oxidative stress, with reduced cellular antioxidant defenses including SOD, is a putative mechanism for pathologic bone loss for many conditions, including estrogen deficiency at menopause (33, 34). Thus this treatment is a potential mitigator for any radiation induced bone loss. Treatment was administered 24 hours following IR and continued twice daily for the duration of the study. The original primary focus of the study was not bone outcomes, but rather pneumonitis and the extent and/or prevention of pulmonary toxicity.

Anesthesia Technique

Each NHP to be irradiated was anesthetized with ketamine (5–15 mg/kg, intramuscular) and dexmedetomidine (0.0075–0.015 mg/kg, intramuscular) and then positioned supine with arms extended overhead. Atipamizole 0.0375–0.075 mg/kg IM was delivered for reversal of dexmedetomidine after irradiation.

Irradiation Technique

A clinical linear accelerator with 6MV photons was used to deliver 10Gy to the anterior-posterior midplane of the thorax of each animal, using a single 6MV x-ray anterior (AP) field and a single 6MV x-ray posterior (PA) field in parallel-opposed, isocentric geometry. Open, rectangular oblong fields (X-Y field size dimensions of 13.0cm (4.0cm, 9.0cm) × 12.0cm) were used without blocking of structures in the thorax with the field central axis placed at the xiphoid. Each field covered the superior aspect of the lungs and included the inferior lung to 4 cm below the xiphoid process. The lateral aspects of each lung and external skin surfaces were included within the radiation fields. The AP field included a 10 to 30 degree wedge (heel superior, angle determined from a computerized tomography (CT) scan of each animal) to compensate for the inferior-to-superior slope of the anterior chest wall, for improved dose homogeneity at midplane. Monitor units (dose delivery settings for the linear accelerator) were calculated assuming homogeneous tissue using measured animal AP diameters, grouping animals into three cohorts by their average AP dimensions.

Each anesthetized animal was placed in the irradiation position and imaged via electronic portal imaging (EPID, iViewGT Amorphous Silicon EPID on a Elekta Infinity Linear Accelerator, 6 MV x-rays) for the AP and then PA fields. The PA field was irradiated first, followed by the AP field (+ wedge) with a nominal dose rate of 6 Gy/min, 5 Gy per field, 10 Gy total to midplane. Each portal imaging procedure, an average of 2 image pairs per IR field, delivered slightly less than 0.02Gy, for a negligible additional dose to the midplane of 0.08 Gy (10.08 Gy total to midplane). A representative dose distribution is shown in Figure 1. All research was approved by the Wake Forest School of Medicine Institutional Animal Care and Use Committee (IACUC).

Imaging and Vertebral Body Segmentation

Total body CT scans were performed for all NHPs at 2 month prior to IR and then at 2, 4, 6, and 8 months following IR. Each CT scan was examined to identify bony pathologies, fractures, and deformities. The thoracic and lumbar vertebrae were segmented from each CT

scan using automated thresholding techniques and manual editing in Mimics (v16.0 Materialise, Leuven, Belgium). Intervertebral disks were excluded and only the bony anatomy was contoured. The vertebral bodies were isolated, and a 3D surface was constructed. The height and diameter of each vertebral body were obtained using measurement tools in Mimics. Each surface was registered to a canonical primate vertebral column using rigid and affine transforms in 3D slicer (v. 3.6, https://www.slicer.org).

Cortical Thickness Analysis

Cortical thickness within each vertebrae was measured using our Ct.Th radiation dose mapping approach (6, 13). Ct.Th was determined at 2000 uniformly distributed vertices along the surface of each vertebral column using Stradwin (v. 5.1 Cambridge, England). The percent change in cortical thickness at homologous vertices was calculated for all scans.

Trabecular Bone Mineral Density Analysis

Similarly, the mean CT density in Hounsfield units (HU) of homologous cylindrical trabecular bone volume in each vertebra was collected in Mimics from multiple slices in each vertebrae roughly 2 – 4 mm apart, excluding end growth plates, and the average HU for each vertebrae was obtained. All scans except six of the pre-irradiation (baseline) scans included a tissue density phantom consisting of materials of known tissue densities, used to convert Hounsfield units into BMD. All scans were performed on the same CT machine and with the same tissue density phantom. For those six baseline scans that did not include the phantom during image acquisition, an average of the data from the scans that included the phantom was used to calculate BMD.

To assess density changes in out-of-field structures, the sarcum and pelvis was segmented using automated thresholding techniques and manual editing in Mimics (v16.0 Materialise, Leuven, Belgium). The average BMD of the pelvis was calculated at baseline and the 4 month time point time and comparisons were made using paired t tests.

Pathologic analysis of bone samples

Vertebral samples from the thoracic and lumbar spine were preserved in 10% neutral buffered formalin for 48 hours prior to storage in 70% ethanol. In preparation for histology, vertebrae were decalcified with a 10% formic acid solution. Specimens were cut in sagittal cross section. Five micrometer representative sections of vertebral bone were cut with a microtome, placed on glass slides and stained with hematoxylin and eosin (H&E).

Statistical analysis

Statistical analysis was performed using R version 3.2.4 software (R Foundation for Statistical Computing, Vienna, Austria). For NHPs that remained until study conclusion, BMD and cortical thickness were compared at all measured time points using repeated measures ANOVA, with Bonferroni post hoc analyses performed for pairwise comparisons. For any NHP removed prior to the conclusion of the study before the 4 month time point, comparisons were made using paired t tests. Toxicity that resulted in removal from the study was compared using a Kaplan Meier analysis.

Results

Eight NHPs were removed from the study between the 2 and 4 month time points due to pulmonary complications; NHPs younger than 50 months old at IR were more prone to a level of pulmonary toxicity that met criteria for a humane endpoint than those older than 50 months at irradiation ($p = 0.03$) as illustrated in Figure 2. Pulmonary effects will be described in a separate report.

A linear regression was performed that compared the BMD and C.Th in NHPs that received hexyl vs saline to determine any radioprotective effects on bone changes; hexyl treatment did not affect the measured bone outcomes as measured by comparing slope of the regression (Figure. 3). Body weight increased from baseline during the follow up period (Figure 4). The mean bodyweight prior to IR was 6.9 kg, and 7.12 kg at time of first follow up. For those NHPs enrolled until the study period, the mean body weight at time of last follow up was 8.27 kg.

For NHPs that remained to the study conclusion, significant loss of Ct.Th in the in-field T9 occurred by 2 months post-IR ($p = 0.0009$), and this loss persisted to 8 months (Figure 5, **Bottom Graphs**). In contrast, no loss of Ct.Th was observed in vertebrae located out-of-field, either L2 or L4. Reduced BMD in these animals was observed by 4 months post-IR for T9 and by 6 months post IR for L2, and L4 ($p < 0.01$; Figure 6). In those NHPs that were removed prior to the study conclusion, both Ct.Th and BMD were lower in T9, L2, and L4 by 2 months post-IR ($p < 0.05$; Figures 5 and 6; **Bottom Graphs**). At an even more distant site, the whole pelvis, BMD was not different at the endpoint for those that were removed from the study prior to conclusion (2 months; $p>0.4$) or in those that remained to study conclusion (8 months; $p>0.08$). Histologically, the regions that exhibited the greatest degree of cortical thinning as determined from CT scans also exhibited increased cortical porosity (Figure 7).

Discussion

As the use of high dose per fraction SBRT becomes more commonplace in modern practice, it is important to understand and quantify the impact of high dose RT on surrounding normal bone both inside and outside the treatment field. During thoracic and lumbar SBRT, bones are commonly exposed to relatively high RT doses (2, 6). Standard fractionation regimens for lung tumors range from 10 to 18 Gy per fraction over a 3 to 5 fraction course (35). In some situations doses up to 34 Gy in a single fraction may be given to lung lesions (36). This unavoidably exposes nearby healthy bone to high doses of radiation per fraction as well. There are currently limited data concerning the acute consequences of high dose per fraction RT to bone. A majority of the pre-clinical literature available has been focused on the late outcomes involving rodent or cell models with fractions of 2 Gy or less (12–15). The limited clinical studies on this topic have shown that thoracic SBRT is associated with changes in bone structural quality directly impacting bone strength. Okoukoni et al. described significant cortical rib thinning in regions receiving ≥ 10 Gy after SBRT (6). Other studies have shown an association between thoracic SBRT and a higher incidence of late rib fractures (approaching 40%) (7–9, 11, 37). Similarly, vertebral SBRT has been associated

with increased progression of VCF (38). Post-mortem analysis of vertebral bodies exposed to SBRT have demonstrated bone fracture, cortical thinning, necrosis, and fibrosis (39). Although the animals treated in this study received radiation to their entire thoracic spine, extrapolation from these data could help shape our expectations of the types of bone changes we should anticipate following more localized treatments like SBRT. Such conformal therapies, can expose one to several vertebral bodies to high doses of radiation per fraction on the order of those used here.

In this study, we observed rapid cortical thinning and trabecular bone loss after whole chest IR to a dose of 10 Gy in 1 fraction in a clinically applicable nonhuman primate (NHP) model. Post-IR pulmonary toxicity was significantly correlated to the age at time of IR where younger NHPs were more sensitive to effects of IR. Approximately 50% of the NHPs were removed due to complications suggestive of pneumonitis, with an average age of 51 months. The average age of those NHPs that lived to the study conclusion was 83 months. Interestingly, this coincides with the age of skeletal maturity (peak BMD) in male rhesus macaques defined as 84 months by Cerroni et al (40).

Animals that died within 4 months post IR experienced rapid persistent bone loss by 2 months post IR throughout the vertebral spine at T9, L2, and L4 in both the trabecular and cortical compartments. Conversely, in those animals that survived to the end of the study, the cortical bone loss was confined to the radiation field only. In these older NHPs that were closer to skeletal maturity at the time of IR, BMD change was noted by 4 months post IR in T9, and by 6 months in L2, and L4. Body weight increased as a function of time post IR ($p=0.005$; Figure 4). Therefore, the observed changes BMD changes were not related to reduced body weight (which is accepted covariate for BMD) (41).

The younger animals in this cohort may have experienced more significant growth and bone turnover than older animals, and their more rapidly growing cells may have been more sensitive to lower doses of RT as well as more pronounced systemic inflammatory effects. The scatter and leakage dose in the lumbar spine, outside the defined IR fields, for these animals was roughly 0.5 – 3% of the dose at the isocenter, which would correlate with doses of roughly 5 – 30 cGy (Figure 1). Doses on the order of 0.5 Gy to 2 Gy have been shown in vivo and in vitro to stimulate an early increase in the number and function of osteoclasts (42–45). In clinical studies, doses as low as 5 Gy have been associated with rapid local bone loss (13). This increased sensitivity of bone in the younger NHPs is also highlighted by the lack of changes in BMD at an even more distant site, the whole pelvis, which received no dose (Figure 1). Thus the dose threshold for bone damage is unclear, but possibly very low. Given that these animals reached a humane endpoint due to pneumonitis related toxicity, some of bone changes observed may have also been related to decreased physical activity.

On histologic analysis trabeculae were qualitatively noted to be unusually thick and oddly shaped in multiple regions throughout the bone, with increased porosity throughout, but also with focal regions of pronounced cortical thickness. Additionally, there was ossification of cartilage above the growth plate and an apparent lack of bone turnover throughout the samples. Empty lacunae were not observed from the vertebrae. While hexyl was not observed to protect against bone loss, the actions of SOD in bone has been shown to have

protective effects on bone osteoprogenitors and osteocytes (33, 34, 46). These histologic findings correlated spatially with thinning identified from quantitative/3D models (Figure 7).

The structural bone changes induced by IR are thought to be the result of multiple physiologic processes affecting osteoblasts, osteoclasts, and bone vascularity (15, 47). Both in vitro and in vivo studies demonstrated that RT directly damages osteoblasts and their precursors leading to impaired matrix production and lower BMD (14, 16, 48). Early up regulation of osteoclast activity leading to rapid bone loss post RT has been reported in rodent models (15, 44, 49). Radiation has been shown to cause an early and substantial increase the expression of pro-osteoclastogenic genes, including Rankl, Mcp1, and TNF-α (44). Young mice irradiated with an acute, large doses comparable to the chest dose in this study (7.25 and 8.0 Gy) exhibited rapid loss of bone (50, 51) coincident with increased systemic biomarkers of TRAP5b (51), a circulating biomarker for osteoclast activity. Additionally, prophylactic use of osteoclast inhibitors have been shown to decrease acute RT induced bone loss in rodents (15). Moreover, exposure of young mice to high dose radiation of 7.25 Gy has been shown to reduce circulating biomarkers of bone formation and osteoblast activity, including sclerostin and procollagen type 1 amino-terminal propeptide (50). Therefore it is likely that the rapid bone loss seen here is facilitated by at least a contribution from both osteoclasts and osteoblasts, though rapid bone loss is likely a feature of elevated osteoclast activity.

This study presents several limitations. As noted, the primary study was examining the protective effects of Hexyl on pulmonary toxicity. In this study, hexyl did not have a protective effect on bone morphology. The cohort of NHPs chosen were based on available samples at the intitation of the study, thus age and weight matching was not possible, however this enabled us to detect that younger NHPs are more radiation sensitive in terms of both bone loss and reaching endpoints associated with pneunonitis. Unfortunately, the sample preparation for the histology permitted H&E staining, but attempts at histochemical staining for osteoclast (TRAP) or osteoblast (ALP) number and activity failed. Thus we are limited to presenting gross observational data.

Conclusion

Rapid and persistent cortical thinning and loss of BMD occurred post-RT in these NHPs. Our data highlights the significance of early radiation induced bone changes and their dependence on both dose and skeletal maturity. Additionally, younger age at IR was associated with greater sensitivity to radiation. These findings should be confirmed on future human trials, however they do present interesting implications for clinical practice, as they illustrate that bone is a radiosensitive tissue. Patients with underlying diagnoses such as osteoporosis or pre-existing VCF may be at increased risk of progression or development of fractures. Avoidance of normal bone in radiation planning may decrease rates of later fractures. Importantly, the rapid rate of bone loss suggests an early increase in osteoclast activity, which is consistent with preclinical studies (15, 44). If such radiation induced changes are primarily due to an early up regulation of osteoclastic activity, then the use of osteoclast inhibitory therapies may provide some degree of bone radioprotection, and identifies the osteoclast as a prime target for therapeutics to prevent the debilitating radiation

therapy-induced fractures in cancer patients. Additionally, the cortical thickness dose mapping approach for measuring subacute bone loss across time as applied in this NHP model can be translated and clinically identify those patients at highest risk for skeletal complications following SBRT.

Acknowledgments

This research was supported by NIH U19 AI67798, NIH T35 OD010946, and NASA NNX15AB50G (JSW)

References

1. Cunha MV, Al-Omair A, Atenafu EG, Masucci GL, Letourneau D, Korol R, et al. Vertebral compression fracture (VCF) after spine stereotactic body radiation therapy (SBRT): analysis of predictive factors. International journal of radiation oncology, biology, physics. 2012; 84(3):e343–9.
2. Rodriguez-Ruiz ME, San Miguel I, Gil-Bazo I, Perez-Gracia JL, Arbea L, Moreno-Jimenez M, et al. Pathological vertebral fracture after stereotactic body radiation therapy for lung metastases. Case report and literature review. Radiation oncology. 2012; 7:50. [PubMed: 22455311]
3. Rordorf T, Hassan AA, Azim H, Alexandru E, Er O, Gokmen E, et al. Bone health in breast cancer patients: a comprehensive statement by CECOG/SAKK Intergroup. Breast. 2014; 23(5):511–25. [PubMed: 24986766]
4. Jawad MS, Fahim DK, Gerszten PC, Flickinger JC, Sahgal A, Grills IS, et al. Vertebral compression fractures after stereotactic body radiation therapy: a large, multi-institutional, multinational evaluation. Journal of neurosurgery Spine. 2016; 24(6):928–36. [PubMed: 26895526]
5. Otani K, Teshima T, Ito Y, Kawaguchi Y, Konishi K, Takahashi H, et al. Risk factors for vertebral compression fractures in preoperative chemoradiotherapy with gemcitabine for pancreatic cancer. Radiotherapy and oncology: journal of the European Society for Therapeutic Radiology and Oncology. 2016; 118(3):424–9. [PubMed: 26806264]
6. Okoukoni C, Lynch SK, McTyre ER, Randolph DM, Weaver AA, Blackstock AW, et al. A cortical thickness and radiation dose mapping approach identifies early thinning of ribs after stereotactic body radiation therapy. Radiotherapy and oncology: journal of the European Society for Therapeutic Radiology and Oncology. 2016; 119(3):449–53. [PubMed: 27072937]
7. Reyngold M, Wu AJ, McLane A, Zhang Z, Hsu M, Stein NF, et al. Toxicity and outcomes of thoracic re-irradiation using stereotactic body radiation therapy (SBRT). Radiation oncology. 2013; 8:99. [PubMed: 23617949]
8. Taremi M, Hope A, Dahele M, Pearson S, Fung S, Purdie T, et al. Stereotactic body radiotherapy for medically inoperable lung cancer: prospective, single-center study of 108 consecutive patients. International journal of radiation oncology, biology, physics. 2012; 82(2):967–73.
9. Amini A, Yeh N, Gaspar LE, Kavanagh B, Karam SD. Stereotactic body radiation therapy (SBRT) for lung cancer patients previously treated with conventional radiotherapy: a review. Radiation oncology. 2014; 9:210. [PubMed: 25239200]
10. Mutter RW, Liu F, Abreu A, Yorke E, Jackson A, Rosenzweig KE. Dose-volume parameters predict for the development of chest wall pain after stereotactic body radiation for lung cancer. International journal of radiation oncology, biology, physics. 2012; 82(5):1783–90.
11. Aoki M, Sato M, Hirose K, Akimoto H, Kawaguchi H, Hatayama Y, et al. Radiation-induced rib fracture after stereotactic body radiotherapy with a total dose of 54–56 Gy given in 9-7 fractions for patients with peripheral lung tumor: impact of maximum dose and fraction size. Radiation oncology. 2015; 10:99. [PubMed: 25897487]
12. Eifel PJ, Donaldson SS, Thomas PR. Response of growing bone to irradiation: a proposed late effects scoring system. International journal of radiation oncology, biology, physics. 1995; 31(5): 1301–7.
13. Okoukoni C, Randolph DM, McTyre ER, Kwok A, Weaver AA, Blackstock AW, et al. Early dose-dependent cortical thinning of the femoral neck in anal cancer patients treated with pelvic radiation therapy. Bone. 2017; 94:84–9. [PubMed: 27780791]

14. Hopewell JW. Radiation-therapy effects on bone density. Medical and pediatric oncology. 2003; 41(3):208–11. [PubMed: 12868120]
15. Willey JS, Livingston EW, Robbins ME, Bourland JD, Tirado-Lee L, Smith-Sielicki H, et al. Risedronate prevents early radiation-induced osteoporosis in mice at multiple skeletal locations. Bone. 2010; 46(1):101–11. [PubMed: 19747571]
16. Mitchell MJ, Logan PM. Radiation-induced changes in bone. Radiographics: a review publication of the Radiological Society of North America, Inc. 1998; 18(5):1125–36. quiz 242–3.
17. Wei RL, Jung BC, Manzano W, Sehgal V, Klempner SJ, Lee SP, et al. Bone mineral density loss in thoracic and lumbar vertebrae following radiation for abdominal cancers. Radiotherapy and oncology: journal of the European Society for Therapeutic Radiology and Oncology. 2016; 118(3): 430–6. [PubMed: 26993414]
18. Seeman E. Is a change in bone mineral density a sensitive and specific surrogate of anti-fracture efficacy? Bone. 2007; 41(3):308–17. [PubMed: 17644058]
19. Treece GM, Gee AH. Independent measurement of femoral cortical thickness and cortical bone density using clinical CT. Medical image analysis. 2015; 20(1):249–64. [PubMed: 25541355]
20. Riseborough EJ, Grabias SL, Burton RI, Jaffe N. Skeletal alterations following irradiation for Wilms' tumor: with particular reference to scoliosis and kyphosis. The Journal of bone and joint surgery American volume. 1976; 58(4):526–36. [PubMed: 178664]
21. Probert JC, Parker BR. The effects of radiation therapy on bone growth. Radiology. 1975; 114(1): 155–62. [PubMed: 813276]
22. Riggs BL, Wahner HW, Dunn WL, Mazess RB, Offord KP, Melton LJ 3rd. Differential changes in bone mineral density of the appendicular and axial skeleton with aging: relationship to spinal osteoporosis. The Journal of clinical investigation. 1981; 67(2):328–35. [PubMed: 7462421]
23. Davies JH, Evans BA, Jenney ME, Gregory JW. Effects of chemotherapeutic agents on the function of primary human osteoblast-like cells derived from children. The Journal of clinical endocrinology and metabolism. 2003; 88(12):6088–97. [PubMed: 14671215]
24. Eastell R. Management of corticosteroid-induced osteoporosis. UK Consensus Group Meeting on Osteoporosis. Journal of internal medicine. 1995; 237(5):439–47. [PubMed: 7738483]
25. Reiter AL, Volk A, Vollmar J, Fromm B, Gerner HJ. Changes of basic bone turnover parameters in short-term and long-term patients with spinal cord injury. European spine journal: official publication of the European Spine Society, the European Spinal Deformity Society, and the European Section of the Cervical Spine Research Society. 2007; 16(6):771–6.
26. Kadan-Lottick N, Marshall JA, Baron AE, Krebs NF, Hambidge KM, Albano E. Normal bone mineral density after treatment for childhood acute lymphoblastic leukemia diagnosed between 1991 and 1998. The Journal of pediatrics. 2001; 138(6):898–904. [PubMed: 11391336]
27. van der Sluis IM, van den Heuvel-Eibrink MM, Hahlen K, Krenning EP, de Muinck Keizer-Schrama SM. Altered bone mineral density and body composition, and increased fracture risk in childhood acute lymphoblastic leukemia. The Journal of pediatrics. 2002; 141(2):204–10. [PubMed: 12183715]
28. Havill LM. Osteon remodeling dynamics in Macaca mulatta: normal variation with regard to age, sex, and skeletal maturity. Calcified tissue international. 2004; 74(1):95–102. [PubMed: 14973638]
29. Black A, Allison DB, Shapses SA, Tilmont EM, Handy AM, Ingram DK, et al. Calorie restriction and skeletal mass in rhesus monkeys (Macaca mulatta): evidence for an effect mediated through changes in body size. The journals of gerontology Series A, Biological sciences and medical sciences. 2001; 56(3):B98–107.
30. Cahoon S, Boden SD, Gould KG, Vailas AC. Noninvasive markers of bone metabolism in the rhesus monkey: normal effects of age and gender. Journal of medical primatology. 1996; 25(5): 333–8. [PubMed: 9029397]
31. Rohrer MD, Kim Y, Fayos JV. The effect of cobalt-60 irradiation on monkey mandibles. Oral surgery, oral medicine, and oral pathology. 1979; 48(5):424–40.
32. Ghandhi SA, Turner HC, Shuryak I, Dugan GO, Bourland JD, Olson JD, et al. Whole thorax irradiation of non-human primates induces persistent nuclear damage and gene expression changes in peripheral blood cells. PloS one. 2018; 13(1):e0191402. [PubMed: 29351567]

33. Yang Y, Zheng X, Li B, Jiang S, Jiang L. Increased activity of osteocyte autophagy in ovariectomized rats and its correlation with oxidative stress status and bone loss. Biochemical and biophysical research communications. 2014; 451(1):86–92. [PubMed: 25063028]
34. Kobayashi K, Nojiri H, Saita Y, Morikawa D, Ozawa Y, Watanabe K, et al. Mitochondrial superoxide in osteocytes perturbs canalicular networks in the setting of age-related osteoporosis. Scientific reports. 2015; 5:9148. [PubMed: 25779629]
35. Timmerman R, Paulus R, Galvin J, Michalski J, Straube W, Bradley J, et al. Stereotactic body radiation therapy for inoperable early stage lung cancer. Jama. 2010; 303(11):1070–6. [PubMed: 20233825]
36. Videtic GM, Hu C, Singh AK, Chang JY, Parker W, Olivier KR, et al. A Randomized Phase 2 Study Comparing 2 Stereotactic Body Radiation Therapy Schedules for Medically Inoperable Patients With Stage I Peripheral Non-Small Cell Lung Cancer: NRG Oncology RTOG 0915 (NCCTG N0927). International journal of radiation oncology, biology, physics. 2015; 93(4):757–64.
37. Asai K, Shioyama Y, Nakamura K, Sasaki T, Ohga S, Nonoshita T, et al. Radiation-induced rib fractures after hypofractionated stereotactic body radiation therapy: risk factors and dose-volume relationship. International journal of radiation oncology, biology, physics. 2012; 84(3):768–73.
38. Rose PS, Laufer I, Boland PJ, Hanover A, Bilsky MH, Yamada J, et al. Risk of fracture after single fraction image-guided intensity-modulated radiation therapy to spinal metastases. Journal of clinical oncology: official journal of the American Society of Clinical Oncology. 2009; 27(30): 5075–9. [PubMed: 19738130]
39. Al-Omair A, Smith R, Kiehl TR, Lao L, Yu E, Massicotte EM, et al. Radiation-induced vertebral compression fracture following spine stereotactic radiosurgery: clinicopathological correlation. Journal of neurosurgery Spine. 2013; 18(5):430–5. [PubMed: 23495889]
40. Cerroni AM, Tomlinson GA, Turnquist JE, Grynpas MD. Bone mineral density, osteopenia, and osteoporosis in the rhesus macaques of Cayo Santiago. American journal of physical anthropology. 2000; 113(3):389–410. [PubMed: 11042540]
41. Willey JS, Grilly LG, Howard SH, Pecaut MJ, Obenaus A, Gridley DS, et al. Bone architectural and structural properties after 56Fe26+ radiation-induced changes in body mass. Radiation research. 2008; 170(2):201–7. [PubMed: 18666808]
42. Goyden J, Tawara K, Hedeen D, Willey JS, Oxford JT, Jorcyk CL. The Effect of OSM on MC3T3-E1 Osteoblastic Cells in Simulated Microgravity with Radiation. PloS one. 2015; 10(6):e0127230. [PubMed: 26030441]
43. Bandstra ER, Thompson RW, Nelson GA, Willey JS, Judex S, Cairns MA, et al. Musculoskeletal changes in mice from 20–50 cGy of simulated galactic cosmic rays. Radiation research. 2009; 172(1):21–9. [PubMed: 19580504]
44. Schreurs AS, Shirazi-Fard Y, Shahnazari M, Alwood JS, Truong TA, Tahimic CG, et al. Dried plum diet protects from bone loss caused by ionizing radiation. Scientific reports. 2016; 6:21343. [PubMed: 26867002]
45. Willey JS, Lloyd SA, Robbins ME, Bourland JD, Smith-Sielicki H, Bowman LC, et al. Early increase in osteoclast number in mice after whole-body irradiation with 2 Gy X rays. Radiation research. 2008; 170(3):388–92. [PubMed: 18763868]
46. Alwood JS, Tran LH, Schreurs AS, Shirazi-Fard Y, Kumar A, Hilton D, et al. Dose- and Ion-Dependent Effects in the Oxidative Stress Response to Space-Like Radiation Exposure in the Skeletal System. International journal of molecular sciences. 2017; 18(10)
47. Kondo H, Searby ND, Mojarrab R, Phillips J, Alwood J, Yumoto K, et al. Total-body irradiation of postpubertal mice with (137)Cs acutely compromises the microarchitecture of cancellous bone and increases osteoclasts. Radiation research. 2009; 171(3):283–9. [PubMed: 19267555]
48. Sams A. The effect of 2000 r of x-rays on the internal structure of the mouse tibia. International journal of radiation biology and related studies in physics, chemistry, and medicine. 1966; 11(1): 51–68.
49. Alwood JS, Shahnazari M, Chicana B, Schreurs AS, Kumar A, Bartolini A, et al. Ionizing Radiation Stimulates Expression of Pro-Osteoclastogenic Genes in Marrow and Skeletal Tissue.

Journal of interferon & cytokine research: the official journal of the International Society for Interferon and Cytokine Research. 2015; 35(6):480–7.

50. Swift JM, Smith JT, Kiang JG. Hemorrhage trauma increases radiation-induced trabecular bone loss and marrow cell depletion in mice. Radiation research. 2015; 183(5):578–83. [PubMed: 25897554]
51. Swift JM, Swift SN, Smith JT, Kiang JG, Allen MR. Skin wound trauma, following high-dose radiation exposure, amplifies and prolongs skeletal tissue loss. Bone. 2015; 81:487–94. [PubMed: 26335157]

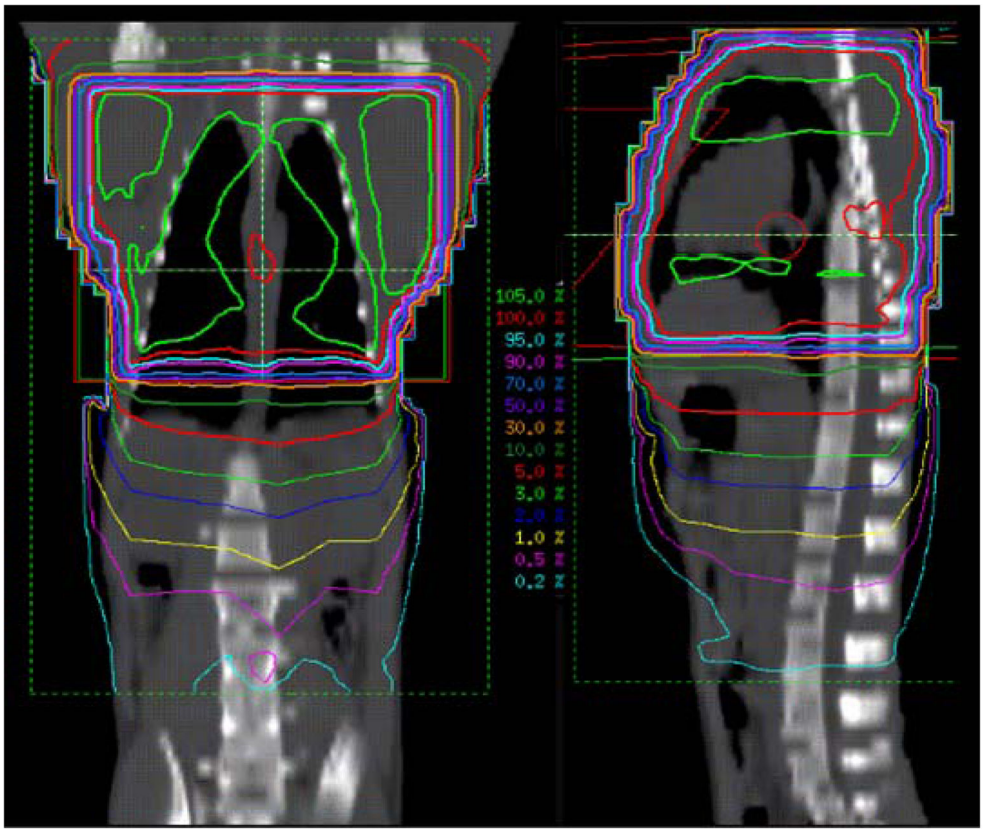

Figure 1.

Two-plane Dose Distributions. Isodose curves in the coronal and sagittal planes for non-human primates (NHPs) receiving chest only radiation to a dose of 10 Gy at the midplane. Note high isodoses, 50 – 105% within the irradiated volume and a gradient of low isodoses, 5 – 0.5%, for the out-of-field volume inferior to the irradiated volume.

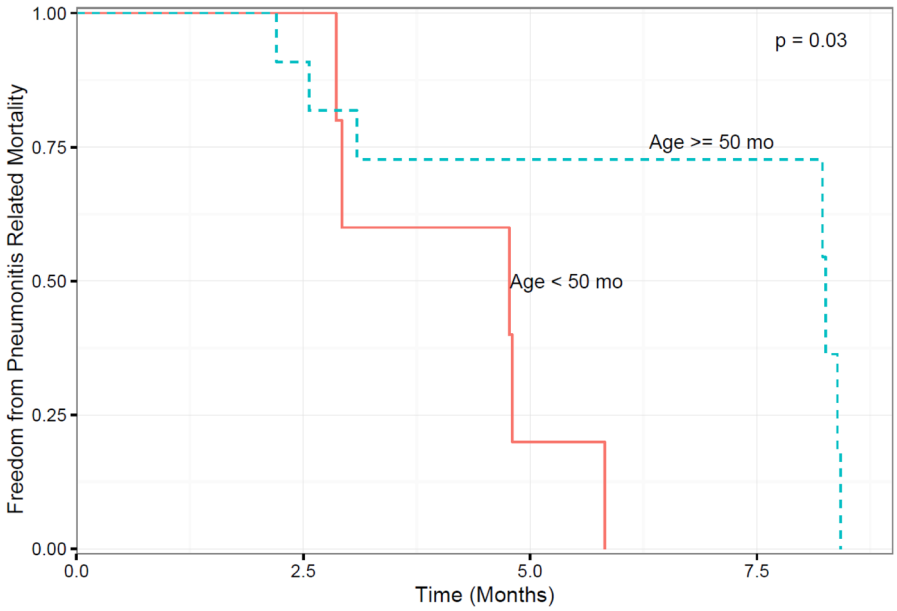

Figure 2.

Kaplan-Meier plot of freedom from pneumonitis related mortality versus time in months after the baseline CT scan (t = 0) for the NHPs, which was taken approximately 2 month prior to irradiation. P = 0.03

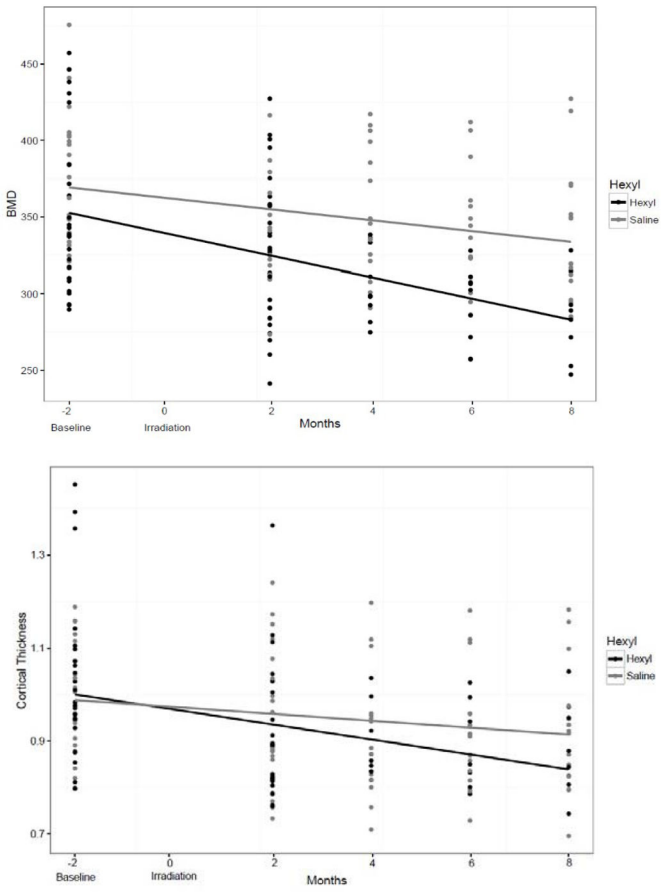

Figure 3.

No protective effect of hexyl on measured bone outcomes. Bone mineral density (Top; BMD) and Cortical Thickness (Bottom; Ct.Th) were plotted using linear regression comparing animals that received hexyl vs saline. Neither test was significant.

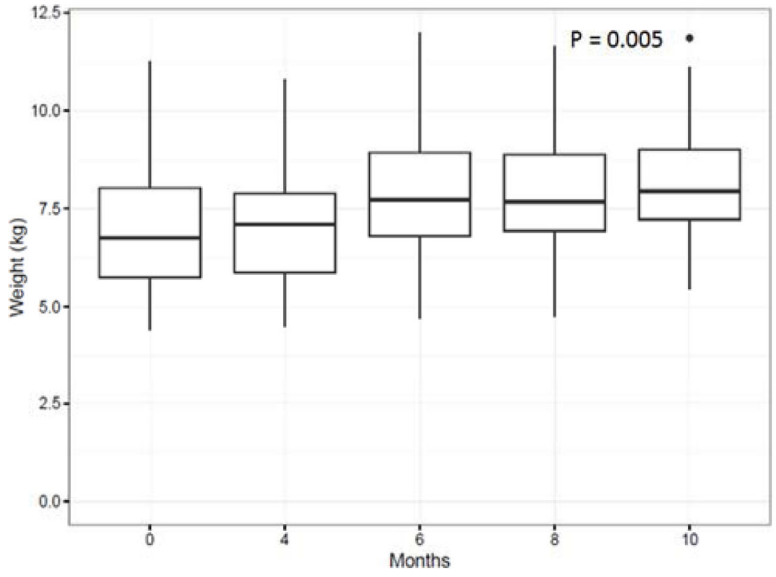

Figure 4.

Body mass increased as a function of time as determined using linear regression (p=0.005). Median body mass (kg) (whiskers 5–95%) as a function of time following the baseline whole body CT scan Chest only irradiation occurred at 2 months after the baseline imaging was performed and this was set to time point t = 0.

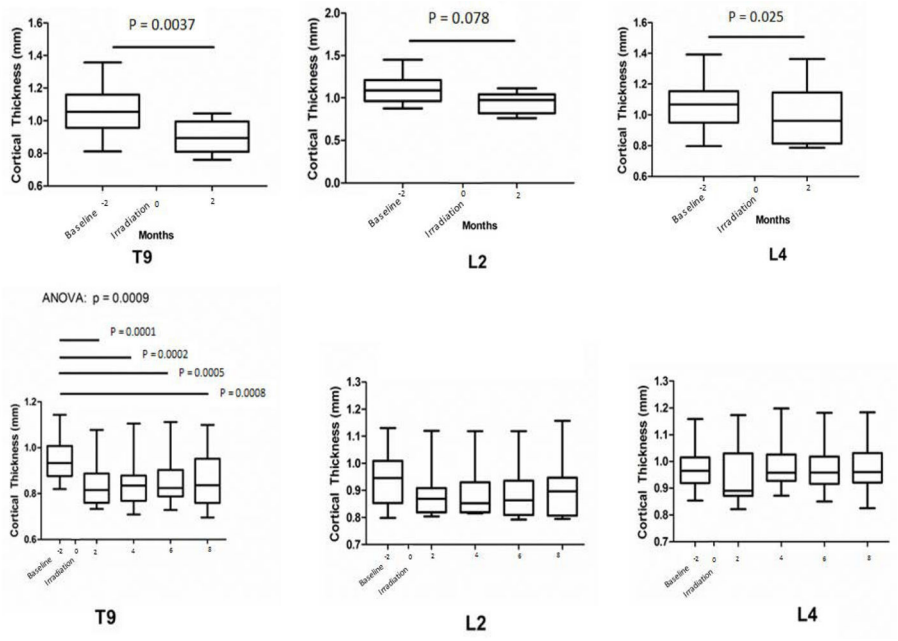

Figure 5.

Median Cortical Thickness (Ct.Th) at the Thoracic (T) and Lumbar (L) vertebrae (whiskers 5–95%) as a function of time (months) following the baseline whole body CT scan in NHPs removed prior to the study conclusion after the 2 month follow-up (**Top**) and in NHPs enrolled to the study conclusion (**Bottom**). Chest only irradiation occurred at 2 month after the baseline imaging was performed and this was set to time point t =0. Paired T test compared Ct. Th for NHPs that were removed prior to study conclusion, while repeated measures ANOVA with Bonferroni post hoc analyses were used for those NHPs that lived to the study conclusion. Bars and associated p values identify significant differences between individual groups; main ANOVA p value presented above graph. The interassay coefficient of variation for each CT-based measure of Ct.Th for those that remained until study conclusion were 10.6–15.0% for T9, 11.1–12.9% for L2, and 9.2–12.4% for L4; and for those that were removed prior to the study conclusion were 10.6–15.2% for T9, 13.1–16.3% for L2, and 16.7–20.0% for L4.

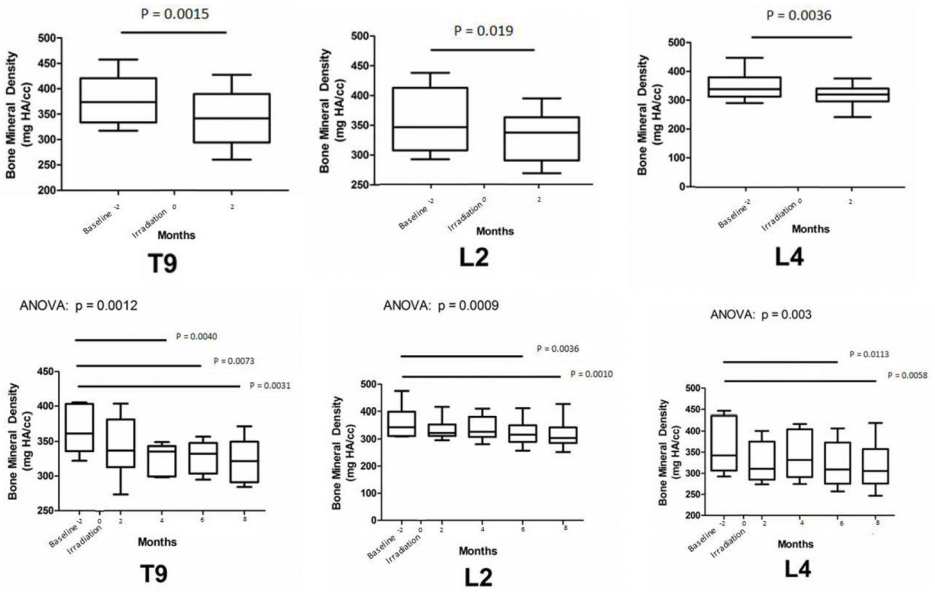

Figure 6.

Median Bone mineral Density (BMD) at the Thoracic (T) and Lumbar (L) vertebrae (whiskers 5–95%) are presented as a function of time (months) following the baseline whole body CT scan in NHPs removed prior to the study conclusion after the 2 month follow-up (**Top**) and in NHPs enrolled to the study conclusion (**Bottom**). Chest only irradiation occurred at 2 month after the baseline imaging was performed and this was set to time point t = 0. Paired T test compared BMD for NHPs that were removed prior to study conclusion, while repeated measures ANOVA with Bonferroni post hoc analyses were used for those NHPs that lived to the study conclusion. Bars and associated p values identify significant differences between individual groups; main ANOVA p value presented above graph. The interassay coefficient of variation for each CT-based measure of BMD for those that remained until study conclusion were 6.7–12.7% for T9, 11.3–16.7% for L2, and 14.6–17.7% for L4; and for those that were removed prior to the study conclusion were 13.3–18.1% for T9, 13.0–15.5% for L2, and 13.2–14.2% for L4.

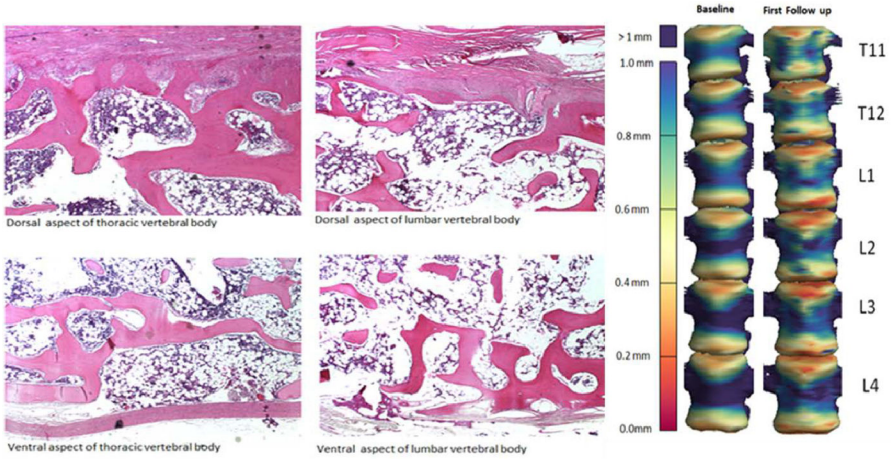

Figure 7.

(Left) Photomicrographs of sagittal sections at the dorsal and ventral aspects of lumbar and thoracic vertebral bodies stained with hematoxylin and eosin (H&E) illustrating lack or severe thinning of cortical bone. (Right) These locations of increased porosity match spatially with the cortical thickness map for thoracic (T) and lumbar (L) vertebrae at time of baseline computed tomography scan (2 months pre IR) versus time of first follow-up imaging (2 months post IR). The cortical thickness (in millimeters) is color coded in the scale to the left of the vertebrae.